SCIENTIFIC REPORTS

OPEN

Facile preparation and adsorption performance of graphene oxide-manganese oxide composite for uranium

Received: 10 January 2018
Accepted: 24 May 2018
Published online: 13 June 2018

Aili Yang[1], Yukuan Zhu[1] & C. P. Huang[2]

To overcome the limits of low adsorption capacity and the separation difficulty of solid from liquid phase for graphene oxide (GO), a novel nanocomposite graphene oxide-manganese oxide (GOMO) was facilely fabricated under ultrasonic radiation. The structures and micro-morphology of the products were characterized by fourier transform infrared (FT-IR) spectroscopy, raman shift spectroscopy, X-ray diffraction (XRD) pattern and scanning electron microscopy (SEM). The effect of solution pH, adsorbent dose, contact time, initial uranium concentration, ionic strength and temperature on uranium removal efficiency was studied by batch adsorption experiments. The product GOMO was used to examine the feasibility of the removal of high salt content in uranium-containing wastewater. The adsorption results were fitted using the Langmuir and Freundlich isotherm models. The kinetic parameters in the adsorption process were measured and fitted. Five adsorption/desorption cycles were performed using 3 M HNO_3 as the regenerant in order to evaluate the reuse of GOMO.

The removal and recovery of nuclide uranium with a long half-life and hazardous radio-toxicity has been regarded as one of the most important and challenging research problems. With the rapid development of various activities related to uranium, most countries have established stringent guidelines for discharge of uranium into water. Therefore, the high-efficiency removal of uranium from aqueous solutions has become a hot research topic[1,2]. Sorption[3–5], which is superior to other techniques (e.g., bioreduction and precipitation[6], reverse osmosis[7], and ion exchange[8,9]), has been widely applied in the wastewater treatment process due to its merits, such as economic, operation simplicity and no secondary pollution. However, most of adsorbents exhibit some disadvantages of low sorption capacity, high cost and lack of environmentally-friendly properties. Therefore, it is very necessary to explore the cheaper and more environmentally friendly adsorbents with higher sorption capacity to meet the current more stringent requirements of water quality and environment protection.

Recently, manganese oxides (Mn_xO_y) have attracted considerable attention owing to their excellent properties (e.g., abundance, environmental friendliness, cheapness and high stability. It has been proven that Mn_xO_y has favourable adsorption action for the removal of heavy metal such as Pb[10], Hg[11], Sr and Co[12]. Nevertheless, Mn_xO_y with fine particle sizes has limited practical application because of its slow solid-liquid separation. Therefore, it is necessary to decorate Mn_xO_y with other large molecular compounds to obtain some superior properties and enhance the practical applications of Mn_xO_y[13].

Graphene oxide (GO) with abundance of oxygen-containing groups (e.g., carboxyl and hydroxyl) has obtained plenty of attention owing to its large specific surface area, excellent adsorption performance and unique electronic properties[14,15]. However, it is well-known that some typical competing cations (e.g., Na^+, K^+, Mg^{2+}, and Ca^{2+}) commonly present in wastewater probably produce a certain interference for the adsorption capacity of GO as the adsorbent. Wan *et al.*[16] reported a nanocomposite graphene oxide-manganese oxide with an outstanding sorption selectivity for Pb(II) when high amounts of Ca(II) coexisted. Moreover, the separation difficulty of the GO-loaded metal ions from liquid phase restricts the practical application of GO. Therefore, it is very valuable to prepare the composites of GO and other substance that combine their advantages. In our previous work we reported the preparation and adsorption performance of the composite GO and chitosan for uranium[17]. To our

[1]Institute of Materials, China Academy of Engineering Physics, Jiangyou, 621907, China. [2]Department of Environmental Engineering, University of Delaware, Newark, DE, 19716, USA. Correspondence and requests for materials should be addressed to A.Y. (email: yang770117@sina.com)

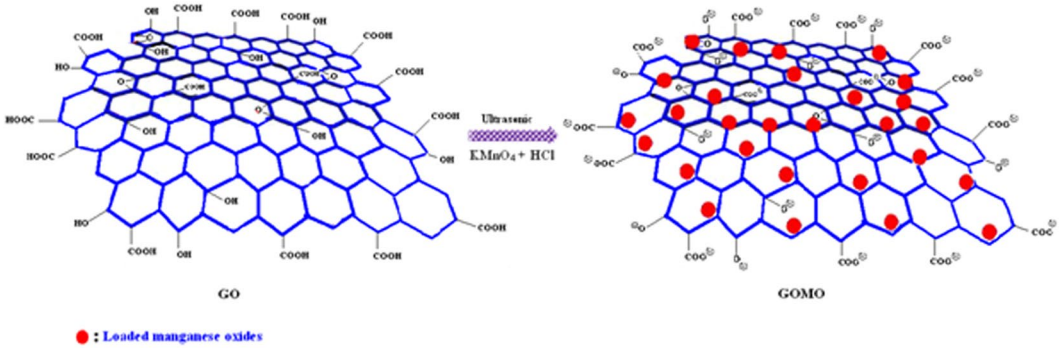

Figure 1. Schematic depiction of the formation of the composite adsorbent GOMO.

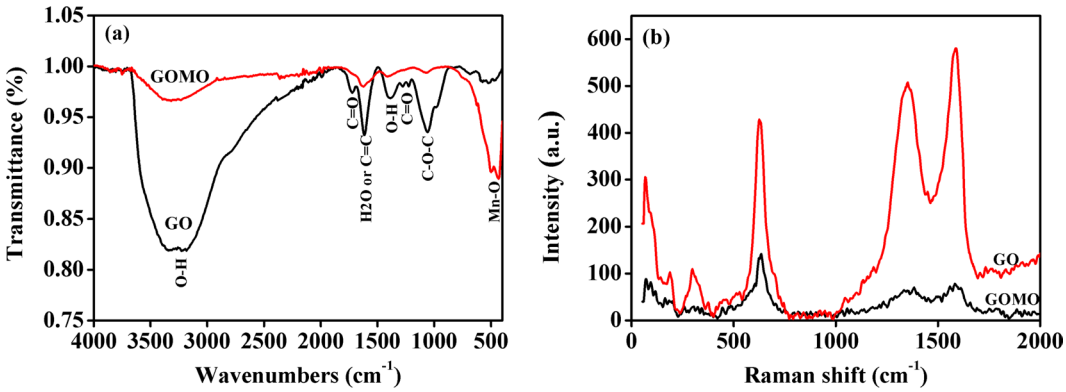

Figure 2. IR spectra (**a**) and raman shift spectra (**b**) of GO and GOMO.

best knowledge, no studies have reported the fabrication of the composite GO/Mn_xO_y under ultrasonic irradiation. Ultrasonic irradiation has been proven to be a highly efficient technique for nanocomposites synthesis because of its advantages of short time, low energy consumption and good shape and size control[18].

Herein, we modified the GO surface with Mn_xO_y by the ultrasonic method and prepared the novel composite adsorbent graphene oxide–manganese oxides (GOMO). The preparation route of GOMO is shown in Fig. 1. The structure and micro-morphology of the products were characterized by FT-IR, raman shift and SEM. The influence of various factors such as pH, sorbent doge, adsorption time, initial uranium concentration, ions strength and temperature on the sorption behaviour of U(VI) onto GOMO from an aqueous solution was investigated. Moreover, the typical industry wastewater with high salinity has been discharged from the nuclear plant which results in the increasing difficulties of nuclear wastewater treatment. Therefore, the feasibility of the removal of high salt content in the wastewater samples using GOMO was also evaluated in this study.

Results and Discussion

Characterization. The FT-IR spectra of GO and GOMO are given in Fig. 2(a). The IR spectrum of GO was similar to that of GO in the reference[19] and showed characteristic peaks at 3345~3229, 1725, 1618, 1387, 1227 and 1061 cm^{-1}, ascribed to O-H stretching vibration, C=O, aromatic C=C, O=C-O and C-O-C stretching vibrations, respectively. However, compared to GO, the characteristic peaks of GOMO assigned to O-H, C=O, C=C and C-O-C were shifted to 3321, 1626, 1413 and 1075 cm^{-1} and the relative peak intensities decreased and in some cases even disappeared. Moreover, the presence of a strong absorption peak at 501 cm^{-1} ascribed to Mn-O vibration and indicated that manganese oxides were loaded successfully onto the surface of GO.

The raman shift spectra of GO and GOMO are presented in Fig. 2(b). Compared to the band of GO, the intensity of the two characteristic peaks of G and D bands in the spectra of GOMO is significantly lower, indicating the formation of the chemical bonds between GO and Mn_xO_y.

In the XRD pattern of Mn_xO_y it was clear that Mn_xO_y was poor crystallized and two broad peaks were observed at 2θ values of 36.7° and 65.7°. Figure 3 showed the XRD patterns of GO (a) and GOMO (b). There were the significant difference between the XRD spectra of GO and GOMO. The XRD analysis of GOMO showed the intensity of all the peaks ascribed to that of stacked GO nanosheets reduced significantly with the increase of the Mn_xO_y amount, suggesting that Mn_xO_y was loaded in the surface of GO. Additionally, two feature diffraction peaks at about 2θ = 36.7° and 65.7° of Mn_xO_y were detected on the composite GOMO (Fig. 3b), indicating the existence of Mn_xO_y on GOMO. Furthermore, by EDS analysis the Mn mass was determined to be 17.40 wt% in GOMO while no Mn element was observed in GO which suggested that the successful combination between GO and Mn_xO_y.

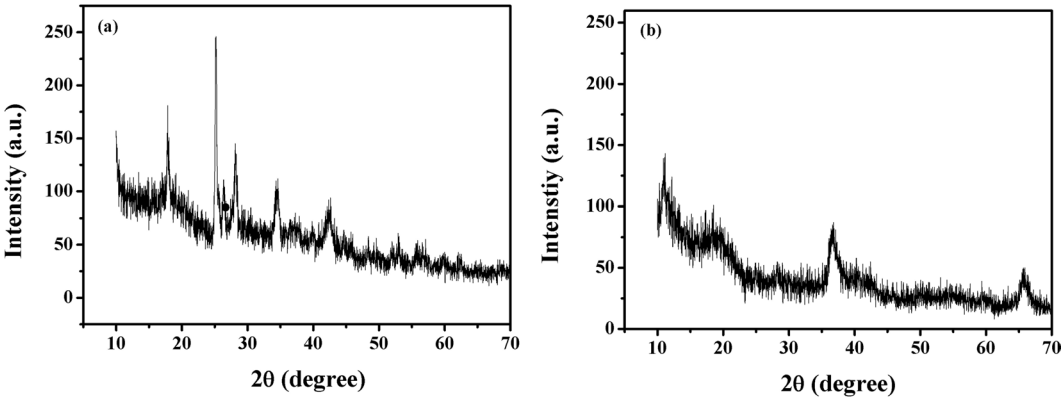

Figure 3. XRD patterns of GO (**a**) and GOMO (**b**).

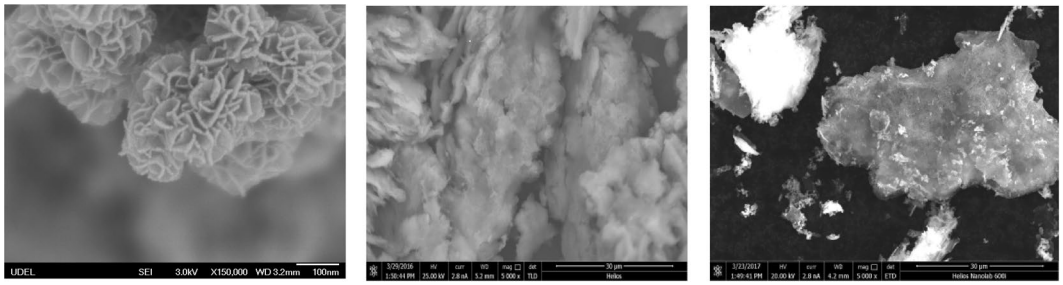

Figure 4. SEM images of Mn_xO_y (**a**), GO (**b**) and GOMO (**c**).

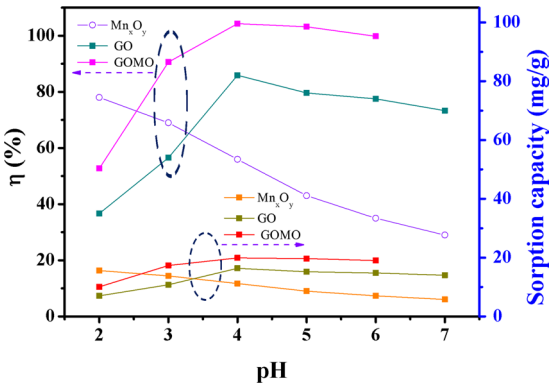

Figure 5. Influence of pH on the adsorption efficiency of uranium by Mn_xO_y, GO, and GOMO. $C_0(U) = 10$ mg/l, adsorbent dosage = 0.5 g/l, T = 298 K, t = 30 min.

Figure 4 shows that micro-morphologies of Mn_xO_y (a), GO (b) and GOMO (c). Both GO and GOMO exhibited lamellar and wrinkled morphology. Moreover, it was seen from Fig. 4(c) that GOMO was covered by a large number of emerging flakes and particles, revealing that Mn_xO_y were attached to the GO surface. Therefore, based on Figs 2, 3 and 4, we can conclude that the composite GOMO was successfully prepared.

Sorption performance. *Influence of solution pH on sorption efficiency.* The removal efficiency of Mn_xO_y, GO and GOMO for U(VI) is presented in Fig. 5 at pH = 2.0–6.0. It was observed that pH had a remarkable influence on the adsorption of U(VI). The removal efficiency increased significantly with increased solution pH. The uranium removal rate of GO and GOMO reached the maximum value (nearly 100%) at pH 4.0. The results showed that the adsorption process depended strongly on the hydrolysed species of U at different pH. The predominant U form was UO_2^{2+} at pH < 4.0, and the adsorption efficiency was low due to the competition between H^+ and UO_2^{2+} for the adsorption sites[20]. $(UO_2)_3(OH)_5^+$ become dominant at pH = 4.5–7.5[21] which resulted in the significant increase of the adsorption efficiency due to electrostatic interaction between $(UO_2)_3(OH)_5^+$ and the GO and GOMO with negative charges. Meanwhile, the adsorption efficiency of GOMO was better than GO.

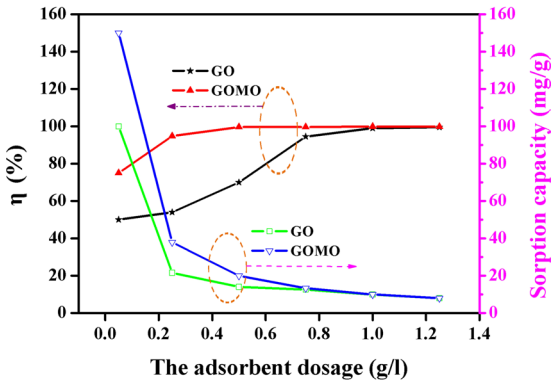

Figure 6. Influence of adsorbent dosage on the sorption efficiency of uranium by GO and GOMO. pH = 4.0, C_0(U) = 10 mg/l, T = 298 K, t = 30 min.

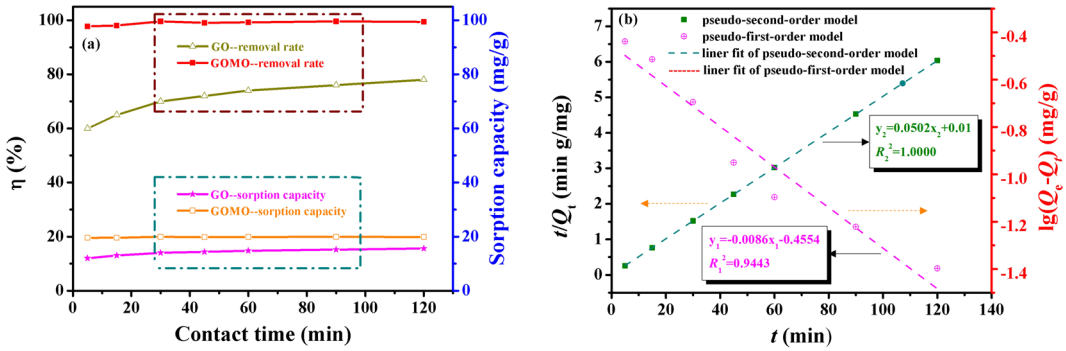

Figure 7. Influence of contact time on uranium sorption of GO and GOMO (**a**) and adsorption kinetics of U(VI) adsorbed by GOMO (**b**). pH = 4.0, C_0(U) = 10 mg/L, adsorbent dosage = 0.5 g/L, T = 298 K.

Kinetic model	T (°C)	c_0 (mg/l)	Q_e (mg/g)	k_1 (g/(mg min))	k_2 (g/(mg min))	R^2
Pseudo-first-order	25	10	0.35	0.0198	—	0.9443
Pseudo-second-order	25	10	19.92	—	0.2520	1.0000

Table 1. Pseudo-first-order and pseudo-second-order model parameters for GOMO.

The results indicated that the doping of Mn_xO_y effectively enhanced the adsorption property of GO. Therefore, pH 4.0 was chosen as the optimum pH.

Influence of adsorbent dosage on sorption efficiency. The influence of adsorbent dosages on sorption efficiency is presented in Fig. 6. The removal efficiency increased sharply when low dosage was used, indicating that there were many readily accessible active sites. With further increase of the dosage, Q_e decreased significantly, while the removal efficiency of uranium shows a steady trend. The maximum removal rate of GO and GOMO reached above 99% when their dosage was 1.0 and 0.5 g/l, respectively. The reason might be fewer available active sites when the adsorption process completed which increases the difficulty of further loading of the adsorbent for uranium ions.

Influence of contact time and kinetic studies. Figure 7 presents the effect of contact time on the sorption of GO and GOMO, and linear fit of sorption kinetic of U(VI) adsorbed by GOMO. It was seen from Fig. 7(a) that GOMO reached favourable removal efficiency (nearly 100%) in a very short time. The sorption reached equilibrium when the surface active sites were saturated and hardly occupied. However, compared to GO the sorption efficiency of GOMO was evidently improved after the modification.

According to Eqs (9) and (10) the calculated parameters of k_1, k_2, Q_e and R^2 are given in Table 1. As seen from Fig. 7(b) the sorption of U(VI) onto GOMO fitted the pseudo-second-order model well ($R^2 = 1.0000$), suggesting that the adsorption of U(VI) onto GOMO was mainly controlled by the chemical process.

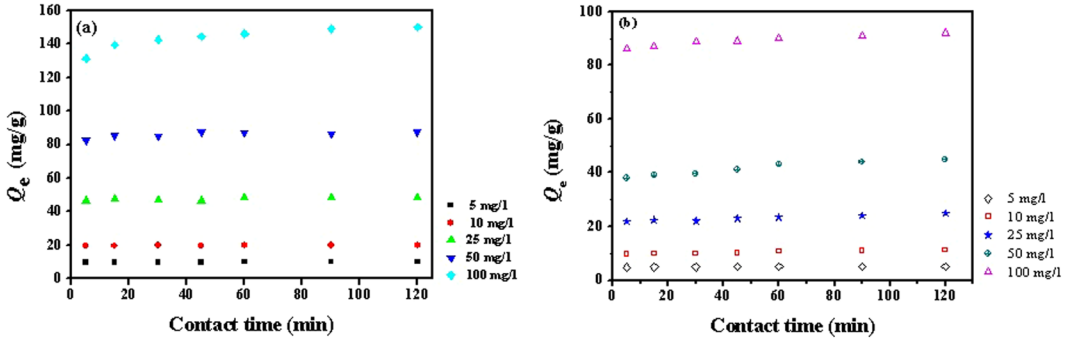

Figure 8. Influence of initial uranium concentration on sorption capacity of GOMO (**a**) and GO (**b**). pH = 4.0, adsorbent dosage = 0.5 g/l, T = 298 K.

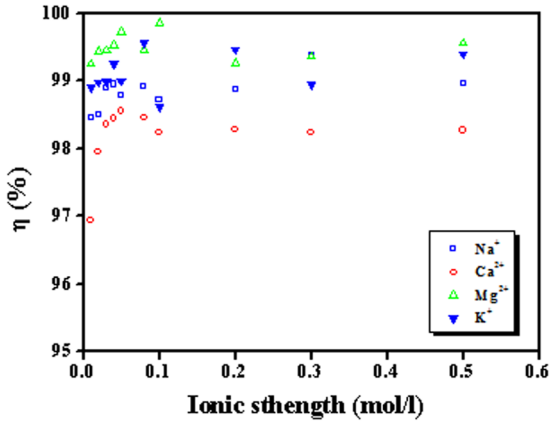

Figure 9. Influence of ionic strength on sorption efficiency of GOMO. pH = 4.0, C_0(U) = 10 mg/l, adsorbent dosage = 0.5 g/l, T = 298 K, t = 30 min.

Influence of initial U(VI) concentration on sorption capacity. The influence of different U(VI) concentrations on the sorption capacity of GOMO is shown in Fig. 8. GOMO had a low sorption capacity at low initial concentrations of <10 mg/l, which was consistent with the findings of Wang *et al.*[22]. However, the sorption capacity of GOMO was significantly elevated and rapidly reached adsorption equilibrium when initial U(VI) concentration increased. The sorption capacity reached above 150 mg/g when the concentration was 100 mg/l. Therefore, it is seen from Fig. 8 that the initial concentration played a significant role in driving U(VI) to adsorb onto the surface of GOMO. Meanwhile, the adsorption capacity presented a very steady trend due to the active sites of GOMO being very rapidly occupied by U(VI) ions and reaching sorption saturation.

Influence of ionic strength on sorption efficiency. Currently, some important cations (e.g., Na^+, K^+, Ca^{2+} and Mg^{2+}) are present universally with relatively high concentrations (>0.2 M) in nuclear waste liquid. However, the ionic-exchange technique depends on high ionic strength and is only suitable for the treatment of uranium-bearing wastewater with the concentration below 0.01 M[23]. To present the applicability of GOMO in the solutions containing varying ionic concentrations (0.01~0.5 M), the effect of ionic strength (Na^+, K^+, Ca^{2+} and Mg^{2+}) on the removal efficiency of uranium was tested. The results are presented in Fig. 9. The results showed that ionic strength did not significantly influence the U(VI) adsorption. Therefore GOMO proved to be a promising adsorbent for nuclear waste liquid even in the presence of very high salinity. The adsorption phenomena generally include inner sphere complexation, outer sphere complexation and ion exchange[24]. Inner sphere complexation is evidently influenced by pH whereas ionic strength will affect outer sphere complexation and ion exchange[25]. Consequently, the uranium adsorption by GOMO was considered to be inner sphere complexation, which was similar with the ref.[26,27].

Adsorption isotherm. Figure 10 shows that linear fit of Langmuir and Freundlich isotherm models of U(VI) adsorbed by GO and GOMO. The Langmuir and Freundlich isotherm parameters are given in Table 2. The adsorption of GOMO and GO fitted Langmuir isotherm model well which indicated that the adsorption process was a monolayer uptake of U(VI) on GOMO and GO. Comparison with GO (Q_m = 16.03 mg/g) shows that the maximum adsorption capacity of GOMO (Q_m = 153.85 mg/g) was improved significantly. Meanwhile, 1/*n* was 0.2815 ($0.1 < 1/n < 0.5$), suggesting that the U(VI) adsorption on the GOMO was favourable.

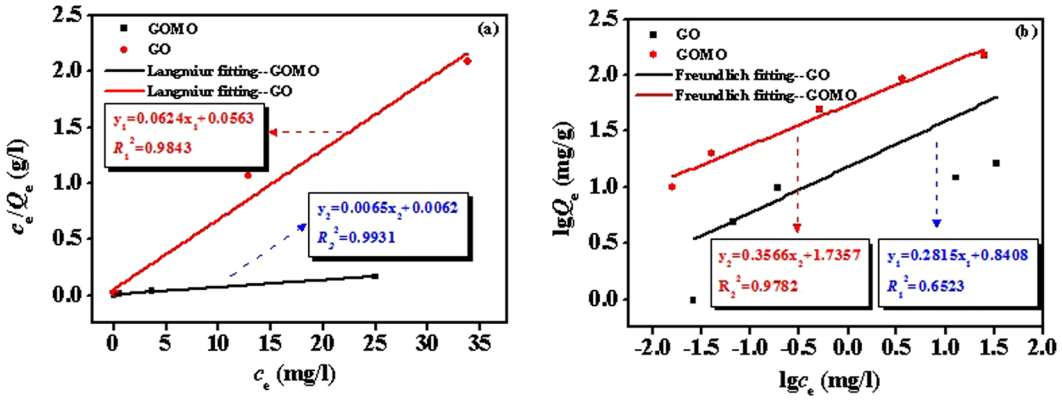

Figure 10. Fitting lines of Langmuir (**a**) and Freundlich (**b**) isotherm models of GO and GOMO.

Adsorbent	Q_m (mg/g)	Langmuir			Freundlich	
		k_L (l/mg)	R^2	n	k_F (mg^{1-n} l^n/g)	R^2
GO	16.03	1.11	0.9843	3.55	6.93	0.6523
GOMO	153.85	1.05	0.9931	2.80	54.41	0.9782

Table 2. Sorption parameters for Langmuir and Freundlich isotherm models.

Sorbents (ref.)	Q_m (mg/g)	Sorbents (ref.)	Q_m (mg/g)
AMGO[34]	123.40	Al_2O_3 nanofibres[35]	204.10
Fe-SC[36]	148.99	Fe_3O_4@TiO_2[37]	118.80
Fe_3O_4/GO[38]	69.49	Layered double oxides/carbon[39]	354.2
Magnetic cucurbit[6]uril/GO[40]	122.50	g-C_3N_4@Ni-Mg-Al-LDH[41]	99.7
Oxime-grafted CMK-5[42]	62.00	*l*-C_3N_4/PDA/PEI_3[43]	60.51
Polyacrylamide–hydroxyapatite[44]	0.95	TiO_{2-x}[45]	65
Polypyrrole[46]	87.72	$CaTiO_x$; $CaAlO_x$[47]	241.7; 258.29
Amidoxime modified Fe_3O_4@SiO_2[48]	105.50	Titanate[49]	358
Modified silica gel[50]	90.30	CNFs[51]	125
Birnessite-modified pine biochar[52]	47.05	p-AO/ CNFs; c-AO/CNFs[53]	588.24; 263.18
Talc[54]	41.60	RUB-15[55]	152
MnO_2–Fe_3O_4–RGO[56]	108.70	GO-CS-P[57]	779.44
SA/CMC-Ca-Al[58]	101.76	Ca/Al-LDH@CNTs[59]	382.9
Phosphate-modified pine wood sawdust[60]	74.10	GO (Present study)	16.03
GOMO (Present study)	153.85		

Table 3. Comparison of the maximum adsorption capacity of various sorbents for uranium at 298 K.

A comparison of Q_m of GO and GOMO in this study and other adsorbents at 298 K is presented in Table 3. It is clear that compared to other listed absorbent, Q_m of GOMO was excellent, suggesting that GOMO shows promising potential for the uranium-bearing wastewater treatment.

Thermodynamic studies. The thermodynamic parameters $\Delta G°$, $\Delta H°$ and $\Delta S°$ were studied from 298 K to 333 K (sorbent dose = 0.5 g/l, C_0(U) = 10 mg/l, V = 20 ml, t = 30 min, pH = 4.0) and were calculated using Eqs (1–3)[28]:

$$K_d = \frac{c_{ad}}{c_e} \tag{1}$$

$$\ln K_d = -\frac{\Delta H^0}{RT} + \frac{\Delta S^0}{R} \tag{2}$$

$$\Delta G^0 = \Delta H^0 - T\Delta S^0 \tag{3}$$

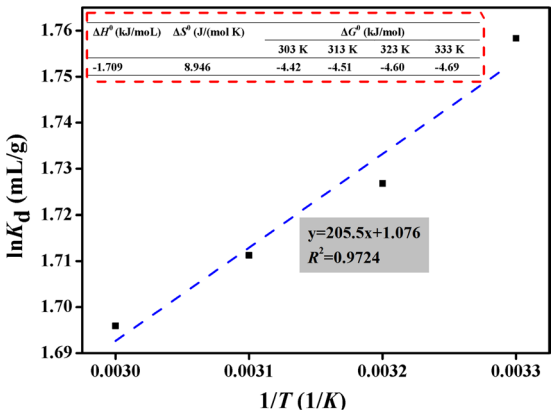

Figure 11. Plot of $\ln K_d$ versus $1/T$ for U(VI) adsorption onto GOMO. pH = 4.0, C_0(U) = 10 mg/l, adsorbent dosage = 0.5 g/l, T = 303 K, 313 K, 323 K and 333 K, t = 30 min. Inset showFigus the thermodynamic parameters of U(VI) adsorption on GOMO.

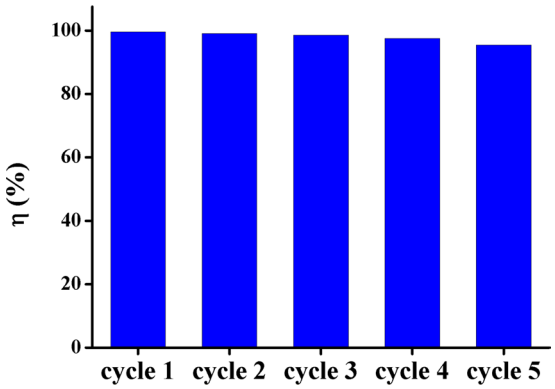

Figure 12. Reusability results for GOMO over five cycles using 3 M HNO_3 as regenerant. pH = 4, C_0(U) = 10 mg/l, T = 298 K, adsorbent dosage = 0.5 g/l.

Where R (8.314 J/(mol·K)) is the universal gas constant, K_d is the sorption equilibrium constant and T (K) is the absolute temperature. The plot of $\ln K_d$ versus $1/T$ for U(VI) adsorption onto GOMO is presented in Fig. 11, and the insert shows the thermodynamic parameters. The negative value of $\Delta H°$ (−1.709 kJ/mol) reflected the fact that adsorption is an exothermic reaction. The positive ΔS^0 and negative ΔG^0 indicated that GOMO was a spontaneous adsorption process. Furthermore, the low absolute values of ΔG^0 and ΔH^0 indicated that the sorption process was physisorption[29].

Regeneration and reuse. Regeneration and cost saving have been very important for the wastewater treatment process. The reuse of GOMO was examined when nitric acid (3 M) was used as the regenerant. The results are presented in Fig. 12. The removal rate of U(VI) could reach 95.45% after five cycles. The results proved that GOMO could be used repeatedly for U(VI) adsorption, and the removal rate of uranium decreased only slightly through five cycles.

Materials and Methods

Materials. Natural graphite was purchased from the Aladdin Chemistry Co. (Shanghai, China). All other chemicals were analytical grade and used without any purification.

Preparation of GOMO. GO were prepared from natural graphite by the modified Hummers method[14]. GOMO was prepared using GO and $KMnO_4$ in the acidic conditions under ultrasonic irradiation. Briefly, GO (0.6 g) in the 40 ml deionized water was sonicated in an ultrasonic bath (Branson 2510, USA) for 2 h in a 250-ml beaker. Then, $KMnO_4$ (0.9 g) and concentrated HCl (2 ml) were added to the suspension of GO. The resulting mixture was sonicated in an ultrasonic bath for 30 min at 60 °C. The precipitates were centrifuged and washed with deionized water and alcohol. Finally, the products were collected and dried at 50 °C under vacuum.

Characterizations. The structures of GO and GOMO were characterized using FTIR spectroscopy (Bruker VERTEX 70, Germany), raman shift spectroscopy (Bruker VERTEX 70, Germany) and X-ray diffraction patterns

(2700 model, China). Scanning electron microscopy (SEM) images of GO and GOMO were obtained using an electron microscope (Helios 600i, Japan).

Adsorption experiments. Standard solutions of uranium (100 μg/ml) were purchased from Chemical Engineering and Metallurgy Research Institute (Beijing, China). The pH of the uranium solutions (20 ml) was adjusted with HCl and NaOH by a pH meter (pHS-25 model, China). The adsorbent was then added to the uranium solution, which was shaken on a shaker (Kangshi, China). After filtration, the residual uranium concentrations were measured by a micro-quantity uranium analyser (MUA model, China). The removal rate η (%) and adsorption capacity at equilibrium Q_e (mg/g) of uranium were calculated using Eqs (4) and (5), respectively:

$$\eta(\%) = \frac{c_0 - c_t}{c_0} \times 100 \tag{4}$$

$$Q_e(mg/g) = \frac{(c_0 - c_e)V}{W} \tag{5}$$

where c_0 and c_t (mg/l) are initial concentration and concentration at time t of U(VI), respectively, c_e (mg/l) is equilibrium concentration of U(VI), W (g) is the adsorbent mass, and V (l) is the solution volume.

Adsorption isotherm. The Langmuir and Freundlich sorption isotherms of GO and GOMO were analysed with different uranium concentrations (5–100 mg/l, $T = 298$ K, sorbent dosage = 0.5 g/l, t = 30 min). The Langmuir isotherm equation[30] assuming the monolayer adsorption process is expressed as follows:

$$\frac{c_e}{Q_e} = \frac{1}{Q_m K_L} + \frac{c_e}{Q_m} \tag{6}$$

$$R_L = \frac{1}{1 + K_L c_0} \tag{7}$$

The Freundlich isotherm[31] is expressed using Eq. (8).

$$\lg Q_e = \lg K_F + \frac{1}{n} \lg c_e \tag{8}$$

where c_e (mg/l) is the concentration at equilibrium, Q_e (mg/g) is the adsorption capacity at equilibrium, Q_m (mg/g) is the maximum adsorption capacity, K_L (l/mg) and K_F ($mg^{1-n}\,l^n/g$) are Langmuir and Freundlich constant, respectively, and n is the Freundlich exponent.

Adsorption kinetics. The pseudo-first-order[32] and pseudo-second-order rate equation[33] are commonly applied to describe the sorption rate and kinetic mechanism, and are expressed using Eqs (9) and (10), respectively:

$$\lg(Q_e - Q_t) = \lg Q_e - \frac{k_1}{2.303} t \tag{9}$$

$$\frac{t}{Q_t} = \frac{1}{k_2 Q_e^2} + \frac{t}{Q_e} \tag{10}$$

Where k_1 (g/(mg·min)) is Lagergren rate constant, Q_e (mg/g) is the adsorption capacity at equilibrium, Q_t (mg/g) is the adsorption capacity at time t, and k_2 (g/(mg·min)) is the pseudo-second-order rate constant.

Regeneration and reuse of GOMO. After adsorption experiments, the obtained U-loaded GOMO was rinsed and washed with 3 M HNO_3 solution and deionized water until no U(VI) was detected in the solution. Then, the regenerated and dried GOMO was reused for further adsorption experiments.

Conclusions

A composite adsorbent GOMO was successfully synthesized by a facile ultrasonic radiation method. GOMO showed high adsorption efficiency for uranium from aqueous solutions at pH = 4.0–6.0. pH significantly influenced the sorption of U(VI) onto GOMO. For the uranium solution of 10 mg/l, the removal of U(VI) reached near completion within 20 min under the sorbent dosage of 0.5 g/l. Compared to GO ($Q_m = 16.03$ mg/g), Q_m of GOMO was improved significantly and reached 153.85 mg/g. GOMO proved to be a promising sorbent for uranium-bearing nuclear wastewater with a high salinity. The sorption data fitted the Langmuir isotherm model and pseudo-second order model well. The adsorption of GOMO for U(VI) proved to be the chemical sorption process. Thermodynamic investigation revealed that U(VI) adsorption onto GOMO was spontaneous and exothermic. The reuse experiments were carried out using 3 M HNO_3, and the sorption efficiency of the regenerated GOMO had only a little decrease after five cycles.

References

1. Li, Z. J. *et al*. Enhanced photocatalytic removal of uranium(VI) from aqueous solution by magnetic TiO_2/Fe_3O_4 and its graphene composite. *Environ. Sci. Technol.* **51**, 5666–5674 (2017).
2. Wang, L. *et al*. Rational control of the interlayer space inside two-dimensional titanium carbides for highly efficient uranium removal and imprisonment. *Chem. Commun.* **53**, 12084–12087 (2017).
3. Tan, L. J. *et al*. Facile preparation of oxine functionalized magnetic Fe_3O_4 particles for enhanced uranium(VI) adsorption. *Colloids Surf. A: Physicochem. Eng. Aspects.* **466**, 85–91 (2015).
4. Lingamdinne, L. P. *et al*. Preparation and characterization of porous reduced graphene oxide based inverse spinel nickel ferrite nanocomposite for adsorption removal of radionuclides. *J. Hazard. Mater.* **326**, 145–156 (2017).
5. Decker, J. D. *et al*. Ship-in-a-bottle CMPO in MIL-101(Cr) for selective uranium recovery from aqueous streams through adsorption. *J. Hazard. Mater.* **335**, 1–9 (2017).
6. Zhang, C., Dodge, C. J., Malhotra, S. V. & Francis, A. J. Bioreduction and precipitation of uranium in ionic liquid aqueous solution by Clostridium sp. *Bioresour. Technol.* **136**, 752–756 (2013).
7. Shen, J. & Schafer, A. Removal of fluoride and uranium by nanofiltration and reverse osmosis: A review. *Chemosphere.* **117**, 679–691 (2014).
8. Sreenivas, T. & Rajan, K. C. Studies on the separation of dissolved uranium from alkaline carbonate leach slurries by resin-in-pulp process. *Separ. Purif. Technol.* **112**, 54–60 (2013).
9. Metwally, S. S., Ahmed, I. M. & Rizk, H. E. Modification of hydroxyapatite for removal of cesium and strontium ions from aqueous solution. *J. Alloy. Compd.* **709**, 438–444 (2017).
10. Zhang, H. *et al*. Removal of aqueous Pb(II) by adsorption on Al_2O_3-pillared layered MnO_2. *Appl. Surf. Sci.* **406**, 330–338 (2017).
11. Xu, H. *et al*. Mn-based perovskite oxides for Hg^0 adsorption and regeneration via a temperature swing adsorption (TSA) process. *Fuel.* **182**, 428–436 (2016).
12. Zhang, L. *et al*. Removal of strontium(II) and cobalt(II) from acidic solution by manganese antimonite. *Chem. Eng. J.* **302**, 733–743 (2016).
13. Pan, N. *et al*. Preparation of graphene oxide-manganese dioxide for highly efficient adsorption and separation of Th(IV)/U(VI). *J. Hazard. Mater.* **309**, 107–115 (2016).
14. Li, Z. J. *et al*. Uranium(VI) adsorption on graphene oxide nanosheets from aqueous solutions. *Chem. Eng. J.* **210**, 539–546 (2012).
15. Cheng, W. C. *et al*. Mutual effect of U(VI) and Sr(II) on graphene oxides: evidence from EXAFS and theoretical calculations. *Environ. Sci. Nano.* **4**, 1124–1131 (2017).
16. Wan, S. *et al*. Rapid and highly selective removal of lead from water using graphene oxide-hydrated manganese oxide nanocomposites. *J. Hazard. Mater.* **314**, 32–40 (2016).
17. Yang, A. L., Yang, P. & Huang, C. P. Preparation of graphene oxide-chitosan composite and adsorption performance for uranium. *J. Radioanal. Nucl. Chem.* **313**(2), 371–378 (2017).
18. Gao, Q. *et al*. Improvement of particles distribution of *in-situ* 5 vol% TiB_2 particulates reinforced Al-4.5Cu alloy matrix composites with ultrasonic vibration treatment. *J. Alloy. Comp.* **692**, 1–9 (2017).
19. Ma, J., Liu, C., Li, R. & Wang, J. Properties and structural characterization of oxide starch/chitosan/graphene oxide biodegradable nanocomposites. *J. Appl. Polym. Sci.* **123**, 2933–2944 (2012).
20. Chen, S., Hong, J., Yang, H. & Yang, J. Adsorption of uranium (VI) from aqueous solution using a novel graphene oxide-activated carbon felt composite. *J. Environ. Radioact.* **126**, 253–258 (2013).
21. Sun, Y. *et al*. The removal of U(VI) from aqueous solution by oxidized multiwalled carbon nanotubes. *J. Environ. Radioact.* **105**, 40–47 (2012).
22. Wang, Z. H., Shen, D. K., Shen, F. & Li, T. Y. Phosphate adsorption on lanthanum loaded biochar. *Chemosphere.* **150**, 1–7 (2016).
23. Ren, J. *et al*. Treatment of high salinity low level radioactive wastewate containing uranium and plutonium by flocculation. *J. Nuclear Radiochem.* **30**(4), 201–205 (2008).
24. Niu, Z. *et al*. Effect of pH, ionic strength and humic acid on the sorption of uranium(VI) to attapulgite. *Appl. Radiat. Isot.* **67**, 1582–1590 (2009).
25. Yu, H. *et al*. Recovery of uranium ions from simulated seawater with palygorskite/amidoxime polyacrylonitrile composite. *Appl. Clay Sci.* **111**, 67–75 (2015).
26. Dolatyari, L., Yaftian, M. R. & Rostamnia, S. Removal of uranium(VI) ions from aqueous solutions using Schiff base functionalized SBA-15 mesoporous silica materials. *J. Environ. Manage.* **169**, 8–17 (2016).
27. Gao, J., Hou, L., Zhang, G. & Gu, P. Facile functionalized of SBA-15 via a biomimetic coating and its application in efficient removal of uranium ions from aqueous solution. *J. Hazard. Mater.* **286**, 325–333 (2015).
28. Guo, X. *et al*. Phosphoryl functionalized mesoporous silica for uranium adsorption. *Appl. Surf. Sci.* **402**, 53–60 (2017).
29. Fan, L., Luo, C., Sun, M., Qiu, H. & Li, X. Synthesis of magnetic-cyclodextrin-chitosan/graphene oxide as nanoadsorbent and its application in dye adsorption and removal. *Colloid. Surf. B Biointerf.* **103**, 601–607 (2013).
30. Langmuir, I. The constitution and fundamental properties of solids and liquids. *J. Am. Chem. Soc.* **38**, 2221–2295 (1916).
31. Freundlich, H. M. F. Uber die adsorption in Iösungen. *Z. Phys. Chem.* **57A**, 385–470 (1906).
32. Lagergren, S. Zur Theorie der sogenannten adsorption geloster stöffe. *K. Sevenska Vetenskapsakad. Handl.* **24**, 1–39 (1898).
33. Ho, Y. & McKay, G. Pseudo-second order model for sorption processes. *Process Biochem.* **34**, 451–465 (1999).
34. Zhao, D. *et al*. Facile preparation of amino functionalized graphene oxide decorated with Fe_3O_4 nanoparticles for the adsorption of Cr(VI). *Appl. Surf. Sci.* **384**, 1–9 (2016).
35. Ren, B. *et al*. Electrospinning synthesis of porous Al_2O_3 nanofibers by pluronic P123 triblock copolymer surfactant and properties of uranium(VI)-sorption. *Mater. Chem. Phys.* **177**, 190–197 (2016).
36. Kong, L. *et al*. Simultaneous reduction and adsorption for immobilization ofuranium from aqueous solution by nano-flake Fe-SC. *J. Hazard. Mater.* **320**, 435–441 (2016).
37. Tan, L. *et al*. Synthesis of Fe_3O_4@TiO_2 core–shell magnetic composites for highly efficient sorption of uranium(VI). *Colloids and Surfaces A: Physicochem. Eng. Aspects.* **469**, 279–286 (2015).
38. Zong, P. *et al*. Synthesis and application of magnetic graphene/iron oxides composite for the removal of U (VI) from aqueous solutions. *Chem. Eng. J.* **220**, 45–52 (2013).
39. Yao, W. *et al*. Synthesis of novel flower-like layered double oxides/carbon dots nanocomposites for U(VI) and ^{241}Am(III) efficient removal: Batch and EXAFS studies. *Chem. Eng. J.* **332**, 775–786 (2018).
40. Shao, L. *et al*. Facile fabrication of magnetic cucurbit[6]uril/graphene oxide composite and application for uranium removal. *Chem. Eng. J.* **286**, 311–319 (2016).
41. Zou, Y. D. *et al*. Synergistic immobilization of UO_2^{2+} by novel graphitic carbon nitride@layered double hydroxide nanocomposites from wastewater. *Chemical Engineering Journal.* **330**, 573–584 (2017).
42. Tian, G. *et al*. Sorption of uranium(VI) using oxime-grafted ordered mesoporous carbon CMK-5. *J. Hazard. Mater.* **190**, 442–450 (2011).
43. Wang, P. Y. *et al*. Superior immobilization of U(VI) and ^{243}Am(III) on polyethyleneimine modified lamellar carbon nitride composite from water environment. *Chem. Eng. J.* **326**, 863–874 (2017).
44. Baybaş, D. & Ulusoy, U. Polyacrylamide–hydroxyapatite composite: Preparation, characterization and adsorptive features for uranium and thorium. *J. Solid State Chem.* **194**, 1–8 (2012).

45. Song, S. *et al*. Simultaneous removal of U(VI) and humic acid on defective TiO_{2-x} investigated by batch and spectroscopy techniques. *Chem. Eng. J.* **325**, 576–587 (2017).
46. Abdi, S. *et al*. Investigation of uranium (VI) adsorption by polypyrrole. *J. Hazard. Mater.* **332**, 132–139 (2017).
47. Hu, Y. Z. *et al*. Superior sorption capacities of Ca-Ti and Ca-Al bimetallic oxides for U(VI) from aqueous solutions. *Chem. Eng. J.* **316**, 419–428 (2017).
48. Zhao, Y. *et al*. Synthesis of amidoxime-functionalized Fe_3O_4@SiO_2 core–shell magnetic microspheres for highly efficient sorption of U(VI). *Chem. Eng. J.* **235**, 275–283 (2014).
49. Yin, L. *et al*. Synthesis of layered titanate nanowires at low temperature and their application in efficient removal of U(VI). *Environ. Pollut.* **226**, 125–134 (2017).
50. Donia, A. M. *et al*. Selective separation of U(VI) from its solutions using amine modified silica gel produced from leached zircon. *Int. J. Miner. Process.* **101**, 81–88 (2011).
51. Sun, Y. B. *et al*. Macroscopic and microscopic investigation of U(VI) and Eu(III) adsorption on carbonaceous nanofibers. *Environ. Sci. Technol.* **50**, 4459–4467 (2016).
52. Wang, S. *et al*. Manganese oxide-modified biochars: preparation, characterization, and sorption of arsenate and lead. *Bioresour. Technol.* **181**, 13–17 (2015).
53. Sun, Y. B. *et al*. Plasma-facilitated synthesis of amidoxime/carbon nanofiber hybrids for effective enrichment of ^{238}U(VI) and ^{241}Am(III). *Environ. Sci. Technol.* **51**, 12274–12282 (2017).
54. Sprynskyy, M. *et al*. Adsorption performance of talc for uranium removal from aqueous solution. *Chem. Eng. J.* **171**, 1185–1193 (2011).
55. Chen, Z. *et al*. Layered silicate RUB-15 for efficient removal of UO_2^{2+} and heavy metal ions by ion-exchange. *Environmental Science Nano.* **4**, 1851–1858 (2017).
56. Tan, L. C. *et al*. The synthesis of a manganese dioxide–iron oxide–graphene magnetic nanocomposite for enhanced uranium(VI) removal. *New J. Chem.* **39**, 868–876 (2015).
57. Cai, Y. W. *et al*. Fabrication of a phosphorylated graphene oxide–chitosan composite for highly effective and selective capture of U(VI). *Environ.Sci. Nano.* **4**, 1876–1886 (2017).
58. Wu, L., Lin, X., Zhou, X. & Luo, X. Removal of uranium and fluorine from wastewater by double-functional microsphere adsorbent of SA/CMC loaded with calcium and aluminum. *Appl. Surf. Sci.* **384**, 466–479 (2016).
59. Chen, H. J. *et al*. Enhanced adsorption of U(VI) and ^{241}Am(III) from wastewater using Ca/Al layered double hydroxide@carbon nanotube composites. *J. Hazard. Mater.* **347**, 67–77 (2018).
60. Zhou, L., Huang, Z. & Luo, T. Biosorption of uranium(VI) from aqueous solution using phosphate-modified pine wood sawdust. *J. Radioanal. Nucl. Chem.* **303**, 1917–1925 (2015).

Acknowledgements

The authors are grateful for financial support from the National Natural Science Foundation of China (21407132).

Author Contributions

Author contributions were as follows: Aili Yang designed the research and wrote the paper. Aili Yang and Yukuan Zhu carried out the experiments. C.P. Huang guided the part work of the experiments.

Additional Information

Competing Interests: The authors declare no competing interests.

Publisher's note: Springer Nature remains neutral with regard to jurisdictional claims in published maps and institutional affiliations.